Available online at www.sciencedirect.com

ScienceDirect

Procedia Computer Science 113 (2017) 400–407

Procedia Computer Science

www.elsevier.com/locate/procedia

The 7th International Conference on Current and Future Trends of Information and Communication Technologies in Healthcare (ICTH 2017)

Augmented Reality Based Brain Tumor 3D Visualization

Qian Shan[a], Thomas E. Doyle[b], Reza Samavi[a,*], Mona Al-Rei[c]

[a]*Department of Computing and Software, McMaster University, 1280 Main St. W, Hamilton, ON, L8S 4L8, Canada*
[b]*Department of Electrical and Computer Engineering, School of Biomedical Engineering, McMaster University, 1280 Main St. W, Hamilton, ON, L8S 4L8, Canada*
[c]*eHealth Graduate Program, McMaster University, 1280 Main St. W, Hamilton, ON, L8S 4L8, Canada*

Abstract

In this paper we present an augmented reality system for mobile devices that facilitates 3D brain tumor visualization in real time. The system uses facial features to track the subject in the scene. The system performs camera calibration based on the face size of the subject, instead of the common approach of using a number of chessboard images to calibrate the camera every time the application is installed on a new device. Camera 3D pose estimation is performed by finding its position and orientation based on a set of 3D points and their corresponding 2D projections. According to the estimated camera pose, a reconstructed brain tumor model is displayed at the same location as the subject's real anatomy. The results of our experiment show the system was successful in performing the brain tumor augmentation in real time with a reprojection accuracy of 97%.

Peer-review under responsibility of the Conference Program Chairs.

Keywords: Augmented reality; 3D visualization; Tumor visualization; Markerless tracking; Mobile device

1. Introduction

Augmented reality (AR) is a type of Mixed Reality (MR) which enhances the physical world by superimposing computer generated images onto it[1]. Such a system allows the user to interact with mixed surroundings of both virtual and physical objects in a natural way. Typically, 2D images are used to exhibit the anatomical structures. In this case, mental mapping is required to match the anatomy with the physical body[2]. Additionally, the left and right orientation are reversed in anatomical images, and the mapping can become confused. However, AR accepts the mental mapping task by overlaying a pre-reconstructed anatomical model directly onto an individual's physical body. This AR system provides a more intuitive approach to visualize the human anatomy and the individual's physical body concurrently. Furthermore, the 3D model provides a potential option to allow the user to view anatomical structures from different directions.

In order to superimpose a computer generated image on its corresponding anatomy, feature tracking is applied to determine the location of the subject. Feature-based tracking techniques can be classified into two groups: marker-

* Corresponding author. Tel.: +1-905-525-9140, ext. 24895
E-mail address: samavir@mcmaster.ca

1877-0509
Peer-review under responsibility of the Conference Program Chairs.
10.1016/j.procs.2017.08.356

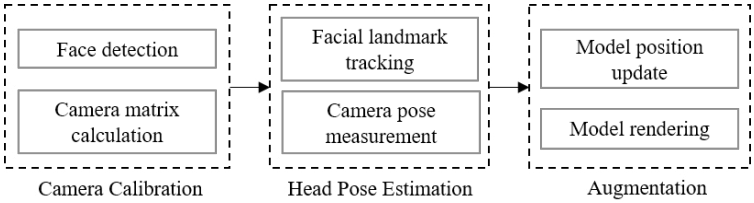

Fig. 1: The proposed system architecture for the AR 3D visualization system

based and markerless tracking[3]. Marker-based tracking uses fiducial markers[4] such as colored dots and QR code, as reference points to assist the system in calculating the camera pose. In markerless tracking, the camera pose is determined from naturally occurring features, such as edges and textures of an anatomical object (e.g. eye corners, nose tip)[5]. A number of medical AR systems reviewed in this paper require excessive preparation to perform marker placement[6] and additional optical tracking systems to track the camera pose[7,8]. Although these systems support a precise accuracy in tracking and overlaying the virtual anatomical model on the patient, placing markers on a patient can be disturbing and the hardware requirements for tracking the markers can be too expensive.

To address the gap in current medical AR systems, we propose a system to augment a pre-reconstructed brain tumor model onto the patient's anatomy using markerless tracking. The system tracks the subject in the scene by using a face detection algorithm. The camera is calibrated based on the face size of the subject. The camera pose is estimated by finding its position and orientation using a collection of facial landmarks and their corresponding 3D points. The model is then rendered at the location of the subject's head according to the estimated camera pose. The system requires no additional tracking devices and can be executed in a more flexible situation as there is no designated environmental setup for running the system. To support portability we prototype our AR system for mobile devices. Our preliminary results show that the system achieved a real-time performance with a reprojection accuracy of 97% and the augmentation manifests no apparent jitter.

The paper is structured as follows: In Section 2 we first describe the system requirements for general AR systems. We then provide an overview of our proposed system and the specifications of its three main components. In Section 3 we describe the experimental procedure and discuss the results of our AR system evaluation on mobile devices. Section 4 describes the related research. We conclude the paper in Section 5 by providing a number of future directions for this research.

2. AR System for Tumor Visualization

In this section, we first describe the requirements for a general AR system and based on these requirements we present our proposed AR system (Section 2.1). Three components of our proposed system architecture are Camera Calibration, Head Pose Estimation, and Augmentation as shown in Fig. 1. In the camera calibration component (Section 2.2), face detection is first applied to find the subject in the scene, and the camera matrix is calculated based on the face size of the subject. Head pose estimation component (Section 2.3) tracks five facial landmarks and their corresponding 3D points to estimate the head pose. The augmentation component (Section 2.4) is responsible for rendering the brain tumor model onto the scene with regard to the position and orientation of subject's head pose.

2.1. Requirements

According to Azuma's survey[9], any AR system should have three major characteristics. First, the system should be able to merge both real and virtual factors. For example, the user should be able to view both the virtual and real objects in the scene through an AR system at the same time. Second, the system must be interactive in real time. For instance, if the user places an object closer to the camera in the real world, the virtual model must respond to the position change simultaneously to match the new scene. Third, the system must provide three-dimensional registration such that the user is able to view the augmented object from more than one direction.

Considering these three characteristics, Zhou *et al*. suggested that a typical augmented reality system is composed of three components which are features tracking, camera pose estimation, and virtual objects rendering and registration[3].

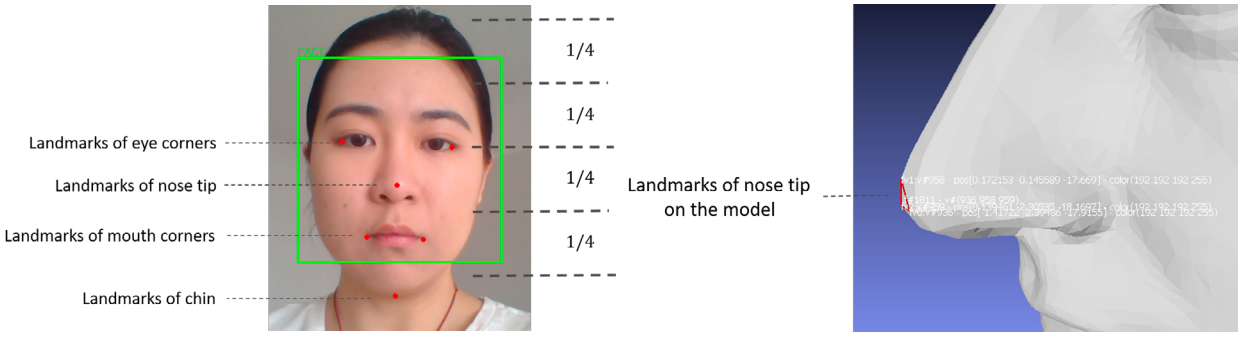

Fig. 2: Facial features extraction. The face is detected within the green rectangle. A human face can be equally divided into four sections. Selected facial landmarks is extracted and marked in red dots (2a). The corresponding 3D landmark points on the model is found using MeshLab (2b).

Fiducial markers such as colored dots, QR code and other featured patterns are commonly used in early AR systems [10,11]. They are considered as a point of reference in feature tracking to find the correspondence between 2D image points and their 3D real world coordinates. Other features also include naturally occurring features such as points, lines or edges [5,12], as well as GPS location for outdoor AR applications [9]. This part ensures the system is interacting with the real world. The camera pose can then be found from projecting the features in 3D coordinates onto the observed 2D image coordinates. Based on the camera pose, the corresponding transformation is applied to the virtual objects to match the viewer's position. This part provides a precise alignment with the real object when rendering the scene.

2.2. Camera Calibration

The camera is calibrated based on pinhole camera model [13,14]. The model is expressed in Eq. 1. The camera matrix, P, is computed using two groups of parameters: extrinsic and intrinsic. The extrinsic parameters consist of a 3x3 rotation matrix R and a 1x3 translation matrix t. This group of parameters presents the transformation from world coordinates to camera coordinates. The intrinsic parameter, K, is expressed as a 3x3 matrix. It consists information of camera focal length, principal point and lens distortion. The focal length (f_x, f_y) is measured in pixels and is defined as the distance between the image plane and focal point with respect to the actual image size. The principal point (c_x, c_y) is located at the intersection point of camera optical axis (usually the z-axis) and the image plane. The lens distortion (s) measures the skewness of the image axes. The formalism as described in Eq. 1 allows the camera coordinates to transform into image coordinates. The resulting 4x3 camera matrix P then maps the 3D world coordinate into the captured image plane. This model can also be extended to perform 3D points projection as shown in Eq. 2. A 3D point in world coordinate (x, y, z) is projected onto the image plane (u, v) based on the rotation and translation of camera axes as well as the camera's intrinsic parameters. This equation is used in Section 2.3 to estimate the subject's head pose.

Typically, the camera calibration is performed using a number of chessboard images. However, it is impractical to ask the user to calibrate the camera using chessboard images whenever the application is installed on a new device. Instead, we implement camera calibration based on Tsai's algorithm [14] by using a set of coplanar points from the image as well as their actual distances. In this paper, we regard the subject's face as a plane and assume there is no lens distortion. The face on the scene is detected using Viola-Jones face detector [15] and an XML classifier from OpenCV [16]. The detector returns the face region as a rectangle and provides a possible width and height of the face in the image as shown in Fig. 2a.

$$P = \begin{bmatrix} R \\ t \end{bmatrix} K, \text{ where } K = \begin{bmatrix} f_x & s & c_x \\ 0 & f_y & c_y \\ 0 & 0 & 1 \end{bmatrix} \quad (1)$$

$$s \begin{bmatrix} u \\ v \\ 1 \end{bmatrix} = K \begin{bmatrix} R \; t^T \end{bmatrix} \begin{bmatrix} x \\ y \\ z \\ 1 \end{bmatrix} \quad (2)$$

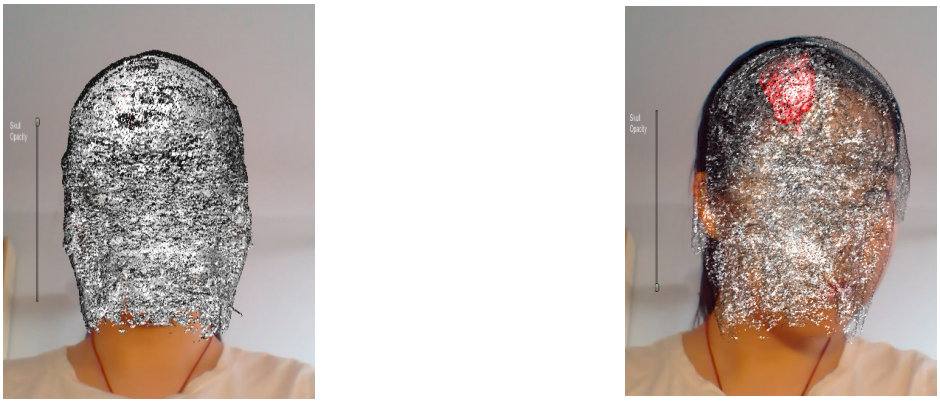

(a) (b)

Fig. 3: The augmentation performance of the system. The brain model is superimposed onto the subject's head (3a). The segmented tumor is highlighted in red color and becomes visible by changing the skull opacity (3b).

In order to obtain a more accurate face size, we also extract the positions of the eyes and nose from the detected face. According to the surface anatomy of the face, the facial features can be equally divided into four sections[17] as shown in Fig. 2a. The first section extends from the apex of the skull to the hair line. The second section is the forehead area. The third section is at the center of the face in proportional length, which is approximately from the eyes to the nasal tip. The last section includes the rest of the face until the chin. We recalculate the face height, from the apex of the skull to the chin, to be fourfold of the vertical distance between eyes and nose. The default face width and height in real world units are set to be the human average values which are 14.8cm and 22.5cm respectively[18]. We also fix the camera's focus mode, so the extrinsic and intrinsic parameters will not change after calibration.

2.3. Head Pose Estimation

The next stage as shown in Fig. 1 is head pose estimation for rendering the right view of the augmented model. The pose of the head represents its relative rotation and translation with respect to the camera[19]. The head pose can be determined by solving a Perspective-n-Problem[20]. The problem aims to determine the camera's position and orientation based on its intrinsic parameters and a collection of corresponding 3D to 2D points. The perspective project model of such a camera is presentsed in Eq. 2. For markerless AR, the most fundamental design challenge is to define the distinct features in the scene as reference points. In this paper, we select a set of 2D landmarks (u, v) of the face, including the corner of both eyes, the nose, the left and right corner of the mouth as well as the chin, using Dlib's facial landmark detector[21] as shown in Fig. 2a. The set of corresponding 3D points (x, y, z) of the same feature are found using MeshLab[22] as shown in Fig. 2b. Since the camera's intrinsic parameters are measured in Section 2.2, we can calculate the rotation and translation vector through solving Eq. 2.

The head pose estimation is only performed when the subject's face is detected in the scene. The resulting rotation and translation values are then applied to the augmented model so that the model is displaying at the same pose as the subject's head.

2.4. Augmentation

The 3D brain model is rendered onto the scene using Unity[23]. The material of the model determines its color and texture. In order to visualize the tumor inside the skull, we apply silver and red color materials to the skull and the tumor meshes respectively. The material for skull mesh is set to be rendered in the transparent mode which allows us to access the alpha channel of the material. The alpha channel contains the material's transparency information and controls the compositing of two overlaid pixels. As shown in Fig. 3b the user is able to visualize the size and location of the tumor by changing the alpha value of the skull's material through user intervention.

The change of head orientation can be tracked and the brain model is rendered in real time at the corresponding view as shown in Fig. 3a and Fig. 3b. We smooth the face tracking process by comparing the current face position with the one detected in the previous frame. If the subject's face has moved within the threshold pixel value, the system will not update the face position. In such a way, the jitter of the augmented model is minimized during visualization.

3. Evaluation

In this section, we describe the experimental procedures for evaluating our proposed system. In Section 3.1 we evaluate the system's accuracy by measuring the reprojection error using an open source face database. In Section 3.2 we evaluate the system's performance by measuring the processing time for each step. Then we discuss the results in Section 3.3.

3.1. Accuracy Experiment

Reprojection error occurs when the points projected by a camera are not perfectly aligned with their original positions[19]. The error is defined to be the Euclidean distance between the original points and their projections. Since the camera intrinsic parameters in Section 2.2 are measured based on the human average face size, it is necessary to test its performance on a representative individual.

A face database of 50 data subjects with a total of 600 images was obtained from the MUCT Face Database[24]. The characteristics of data subjects are described in Table 1. All data subjects are 18 years or more of age and having a variety in cultural background. The gender is equally distributed within the database. Each of the data subjects is imaged at four different camera views (A to D) under three different lighting conditions. At position A, the camera is placed directly in front of the subject, 40 degrees to the right at position B, and about 20 degrees above and below the subject at position C and D respectively. The lighting condition is classified into three groups: low, normal and flashlight. Each group exhibits a mean luminance of 86, 104 and 146 accordingly. Each possible feature value except for the glasses is uniformly represented in the database in order to avoid the bias towards particular conditions.

Table 1: Each subject in the database is labeled with five main features

Feature	Range	Distribution
Age	18 and older	
Gender	Male, Female	50% / 50%
Camera View	A - front	25%
	B - 40 degrees right	25%
	C - 20 degrees above	25%
	D - 22 degrees down	25%
Lighting Condition	L - low lighting	33%
	N - normal lighting	33%
	F - Flashlight	33%
Glasses	Yes, No	30% / 70%

Table 2: The mean and standard deviation of measured reprojection error

Lighting Setup	Mean	Standard Deviation
With Glasses		
Low lighting	29.4	10.5
Normal lighting	28.1	9.4
Flashlight	27.5	8.5
Without Glasses		
Low lighting	26.0	9.2
Normal lihting	25.4	8.6
Flashlight	24.1	8.1

We selected the same five facial landmarks as we did in Section 2.3 for this test. The coordinates of the reprojected facial landmark points were calculated by projecting their corresponding 3D points to the 2D image coordinates using the intrinsic parameters. We calculated the intrinsic parameters for each subject based on the subject's face at position A, the frontal view. The reprojection error was assessed using images at the other three camera views. This procedure was then repeated for every light setting, and the reprojection error results are shown in Fig. 4 and Table 2. The mean and standard deviation of the measured reprojection errors are presented in Table 2. The distribution of reprojection error is illustrated in Fig. 4. The majority of the data subjects receives a reprojection error of 25 pixels. This reprojection error is compared with the image's diagonal resolution to measure the reprojection accuracy. The image's diagnonal resolution in pixels is considered as the accepted maximum reprojection error distance. The percentage accuracy is calculated by dividing the difference between the measured and accepted maximum reprojection error by

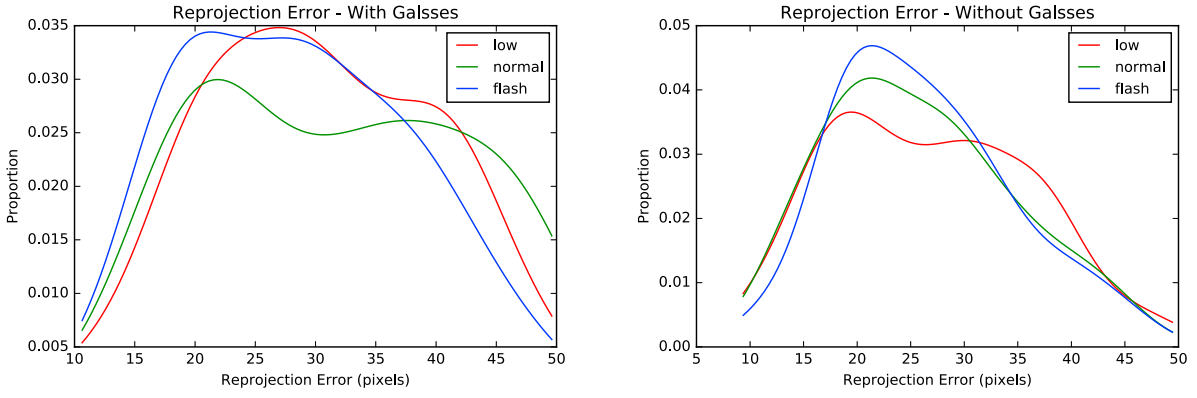

(a) (b)

Fig. 4: The distribution of reprojection error under three light settings for subjects who are wearing glasses (4a) and without glasses (4b).

the accepted maximum error value. The lighting condition can affect the reprojection accuracy to some extent, as the frequency of having higher reprojection error increases under poor lighting condition. The mean reprojection error reduces 2 pixels, and a lower standard deviation is obtained when the subject is imaged under flashlight compared to when the subject is imaged under low lighting condition. Fig. 4a shows the error results for data subjects who wear glasses. More data subjects receive a higher reprojection error and the standard deviation also become larger when he/she is wearing a glasses. However, the error can be reduced under a better lighting condition.

3.2. Performance Experiment

In the second experiment, we measured the required processing time for each step to evaluate its performance individually. All the experiments are executed on the Android cell phone with an Octa-Core@1.5GHz 3GB RAM. The volumetric MRI data used for testing is obtained from The Cancer Image Archive (TCIA)[25], and the face section is removed to protect the privacy of data subjects.

We performed the test with two models which were reconstructed from datasets of different resolutions. The resolution of two brain models are shown in the first column. The following three columns present the processing time for each step. We measured the processing time in both millisecond (ms) and frame per second (FPS) units. The last column in Table 3 represents the combined processing time for both head pose tracking and model rendering since these two steps are always executed in sequence and the combined processing time better represents the real performance of the system. The model reconstructed from higher resolution dataset lowers the overall system processing speed and it takes the system seven more milliseconds to perform tracking and rendering tasks. As the camera is set to provide the texture at 30 FPS, the system is still able to process every frame coming from the camera. Therefore, we can conclude that our system runs in real time.

Table 3: Measured processing time for each step with medical image datasets of different dimensions

Dataset Resolution	**Camera Calibration**	**Head Pose Tracking**	**Rendering**	**Tracking plus Rendering**
216x256x160	23 ms	10 ms	5 ms	15 ms
	43 FPS	100 FPS	200 FPS	66 FPS
512x512x176	25 ms	14 ms	8 ms	22 ms
	40 FPS	71 FPS	125 FPS	45 FPS

3.3. Discussion

The two experiments demonstrate the system successfully augments the virtual brain model onto the subject's head in real time, manifesting an average reprojection accuracy of 97% with little or no apparent jitter. The system is sensitive to lighting conditions. A better accuracy can be achieved under a decent light setting and without wearing any face accessories. The system also allows the users to view the size and location of segmented tumor through user intervention.

The system still exhibits some limitations. Despite the fact that the system supports tracking for 6 degrees of freedom movement, our investigation shows the head rotation is limited to approximately 40 degrees since certain facial features will disappear from the scene when rotating beyond this degree. The 25 pixels reprojection error is tolerable through visual assessment, but it can lead to huge deviation in surgical environment. In this case, a more precise camera calibration procedure will be required. Since the camera on most cell phones does not capture any depth information, this application does not support occlusion. The virtual brain model therefore will always appear at the closest layer of the scene.

4. Related Work

Multiple commercial products are currently available for visualizing human anatomy in a three-dimensional manner, such as Anatomage Table[26] and Cyber-Anatomy[27]. Both of them offer 3D anatomy models which are segmented with the real human. As these devices do not support video-see-through to interact with the reality, the users will not be able to view the anatomical structures as a part of their bodies. An improvement on these visualization products are systems such as the Ablation Guidance Tool[6] and Hydride In-Situ Visualization[7]. Nicolau *et al.* proposed a marker based AR guidance tool for assisting radio-frequency ablation. Before running their system, the patient requires to take CT scans with twenty-five frequency-opaque markers on their skin. In augmentation process, the precise alignment is achieved by matching the markers on the CT scans with the ones on the patient. Bichlmeier's In-Situ Visualization uses two tracking systems, inside-out and outside-in tracking system, to track the fiducial makers in both the see-through head mounted device (HMD) as well as the real working area. The registration of virtual and real objects is achieved by converting both coordinates from two tracking systems to the reference frame.

Markerless AR is also available in medical field. Mirracle[8] is proposed to be magic mirror for assisting anatomy education. The system augments a volumetric skeleton CT dataset onto the user. The pose of the user is tracked using the NITE skeleton tracking system[28]. In addition, Cukovic *et al.* proposed a system to visualize 3D foot phantoms[29]. Their system generates a descriptor for every camera image. The descriptor includes a set of feature points and the dominant keypoint orientation. Their system tracks the real world object by matching the descriptor from the live video with those in their database. However, this method only supports tracking of limited number of objects.

Mobile phones have been shown to have the computational power to support 3D medical volumetric data visualization. Mairer-Hein *et al.* presented a markerless AR system to visualize 3D medical images on portable devices[30]. The system used a mounted Time-of-Flight camera to generate a surface of the object in the scene and the object tracking demonstrates to operate at 10 FPS. The camera pose was computed by matching the surface to its corresponding image dataset using iterative closest point algorithm.

Most of the current AR systems use fiducial markers and requires special purpose equipment for object tracking. It needs excessive time to set up the environment and is limited to a particular working area (e.g. an fully equipped operating room or laboratory). The markerless AR applications do not perform in real time, due to the expensive computational cost for tracking an object and rendering the virtual model. Our proposed system will improve upon existing AR visualization systems by using a pre-reconstructed 3D model to perform 3D visualization on a mobile device in real time.

5. Conclusions and Future Work

In this paper, we have demonstrated an AR system for visualizing 3D brain tumor model. The proposed system is based on the face detection algorithm which detects and tracks an subject in the scene. Such a system will assist physicians and the patients by providing a more intuitive visualization on the location and size of the tumor. The

system successfully overlaid the brain model onto the patient's head and achieved a real-time performance on the mobile device. We will further evaluate this system with real patients and compare the usage with common 2D medical scans. Furthermore, considering that there is limited information we can obtain from most of the mobile device cameras, we are planning to build our system on Microsoft HoloLens[31]. The locatable camera on HoloLens captures its location information with respect to the physical world, which allows our system to provide a more powerful visualization such as a various visualization direction and zoom-in option to view more details of a tumor.

References

1. Carmigniani, J., Furht, B., Anisetti, M., Ceravolo, P., Damiani, E., Ivkovic, M.. Augmented reality technologies, systems and applications. Multimedia Tools and Applications 2011;51:341–377.
2. Macedo, M.C.F., Jr., A.L.A., Souza, A.C.S., Giraldi, G.A.. A semi-automatic markerless augmented reality approach for on-patient volumetric medical data visualization. In: Virtual and Augmented Reality (SVR). 2014,.
3. Zhou, F., Duh, H.B.L., Billinghurst, M.. Trends in augmented reality tracking, interaction and display: A review of ten years of ismar. In: ISMAR '08. 2008, p. 193–202.
4. Kan, T.W., Teng, C.H., Chou, W.S.. Applying QR code in augmented reality applications. In: Proceedings of the 8th International Conference on Virtual Reality Continuum and its Applications in Industry. ACM; 2009, p. 253–257.
5. Vacchetti, L., Lepetit, V., Fua, P.. Combining edge and texture information for real-time accurate 3d camera tracking. In: ISMAR '04. 2004, p. 48–57.
6. Nicolau, S.A., Pennec, X., Soler, L., Ayache, N.. An augmented reality system to guide radiofrequency tumour ablation. Computer Animation and Virtual Worlds 2005;16:1–10.
7. Bichlmeier, C., Wimmer, F., Heining, S.M.. Contextual anatomic mimesis hybrid in-situ visualization method for improving multi-sensory depth perception in medical augmented reality. In: ISMAR '07. 2007,.
8. Blum, T., Kleeberger, V., Bichlmeier, C.. mirracle: An augmented reality magic mirror system for anatomy education. In: Virtual Reality Short Papers and Posters. 2012,.
9. Azuma, R.T.. A survey of augmented reality. Teleoperators and Virtual Environments 1997;6:355–385.
10. Cho, Y., Lee, J., Neumann, U.. A multi-ring color fiducial system and an intensity-invariant detection method for scalable fiducial-tracking augmented reality. In: In IWAR. 1998, p. 147–165.
11. Naimark, L., Foxlin, E.. Circular data matrix fiducial system and robust image processing for a wearable vision-inertial self-tracker. In: ISMAR '02. 2002, p. 27–36.
12. Comport, A.I., Marchand, E., Chaumette, F.. A real-time tracker for markerless augmented reality. In: ISMAR '03. 2003, p. 36–45.
13. Zhang, Z.. A flexible new technique for camera calibration. IEEE Transactions on Pattern Analysis and Machine Intelligence 2000;22:1330–1334.
14. Tsai, R.Y.. A versatile camera calibration technique for high-accuracy 3d machine vision metrology using off-the-shelf tv cameras and lenses. IEEE Journal on Robotics and Automation 1987;3:323–344.
15. Viola, P., Jones, M.J.. Robust real-time face detection. International Journal of Computer Vision 2004;57:137–154.
16. Bradski, G.. Opencv. Dr Dobb's Journal of Software Tools 2000;.
17. Broadbent, T.R., Mathews, V.L.. Artistic relationships in surface anatomy op the face: Application to reconstructive surgery. Plastic and Reconstructive Surgery 1957;20:1–17.
18. Ahlstrom, V., Longo, K.. Human factors design standard (hf-std-001). Tech. Rep.; Federal Aviation Administration; William J. Hughes Technical Center, Atlantic City International Airport, NJ; 2003.
19. Shapiro, L.G., Stockman, G.C.. Computer Vision. Prentice Hall; 2001.
20. Lepetit, V., Moreno-Noguer, F., Fua, P.. Epnp: An accurate o(n) solution to the pnp problem. International Journal of Computer Vision 2009;.
21. King, D.E.. Dlib-ml: A machine learning toolkit. Journal of Machine Learning Research 2009;10:1755–1758.
22. Cignoni, P., Callieri, M., Corsini, M., Dellepiane, M., Ganovelli, F., Ranzuglia, G.. MeshLab: an Open-Source Mesh Processing Tool. In: Scarano, V., Chiara, R.D., Erra, U., editors. Eurographics Italian Chapter Conference. The Eurographics Association. ISBN 978-3-905673-68-5; 2008,doi:10.2312/LocalChapterEvents/ItalChap/ItalianChapConf2008/129-136.
23. Unity technologies. 2017. URL: `https://unity3d.com`; accessed: 2017-05-15.
24. Milborrow, S., Morkel, J., Nicolls, F.. The muct landmarked face database. Pattern Recognition Association of South Africa 2010;, http://www.milbo.org/muct.
25. Cancer image archive. 2017. URL: `http://www.cancerimagingarchive.net/`; accessed: 2017-05-15.
26. Anatomage table. 2016. URL: `http://www.anatomage.com/table/`; accessed: 2017-05-27.
27. Cyber-anatomy. 2014. URL: `https://www.cyber-anatomy.com/`; accessed: 2017-05-27.
28. Openni. 2013. URL: `http://openni.ru/files/nite/`; accessed: 2017-05-27.
29. Cukovic, S., Gattullo, M., Pankratz, F., Devedzic, G., Carrabba, E., Baizid, K.. Marker based vs. natural feature tracking augmented reality visualization of the 3d foot phantom. In: The Second International Conference on Electrical and Bio-medical Engineering. 2016,.
30. Maier-Hein, L., Franz, A.M., Fangerau, M., Schmidt, M., Seitel, A., Mersmann, S., et al. Towards mobile augmented reality for on-patient visualization of medical images. Bildverarbeitung fur die Mediz 2011;:389–393.
31. Microsoft hololens. 2017. URL: `https://www.microsoft.com/en-us/hololens`; accessed: 2017-05-28.